

# BASIC PRINCIPLES OF SOLAR ACOUSTIC HOLOGRAPHY

(Invited Review)

C. LINDSEY and D. C. BRAUN<sup>\*,†</sup>

*Solar Physics Research Corporation, 4720 Calle Desecada, Tucson, AZ 85718, U.S.A.*  
(e-mails: *lindsey@sprc.com; dbraun@solar.stanford.edu*)

(Received 5 October 1999; accepted 2 February 2000)

**Abstract.** We summarize the basic principles of holographic seismic imaging of the solar interior, drawing on familiar principles in optics and parallels with standard optical holography. Computational seismic holography is accomplished by the phase-coherent wave-mechanical reconstruction of the  $p$ -mode acoustic field into the solar interior based on helioseismic observations at the solar surface. It treats the acoustic field at the solar surface in a way broadly analogous to how the eye treats electromagnetic radiation at the surface of the cornea, wave-mechanically refocusing radiation from submerged sources to render stigmatic images that can be sampled over focal surfaces at any desired depth. Holographic diagnostics offer a straight-forward assessment of the informational content of the observed  $p$ -mode spectrum independent of prospective physical models of the local interior anomalies that it represents. Computational holography was proposed as the optimum approach whereby to address the severe diffraction effects that confront standard tomography in the solar  $p$ -mode environment. It has given us a number of remarkable discoveries in the last two years and now promises a new insight into solar interior structure and dynamics in the local perspective. We compare the diagnostic roles of simple acoustic-power holography and phase-sensitive holography, and anticipate approaches to solar interior modeling based on holographic signatures. We identify simple computational principles that, applied to high-quality helioseismic observations, make it easy for prospective analysts to produce high-quality holographic images for practical applications in local helioseismology.

## 1. Introduction

In the past two years, the application of seismic holography to helioseismic data from the Solar Heliospheric Observatory (SOHO) spacecraft has uncovered a remarkable array of new solar acoustic phenomena. These have included the discoveries of ‘acoustic moats’ surrounding sunspots (Lindsey and Braun, 1998a; Braun *et al.*, 1998), apparent ‘acoustic condensations’ 10–20 Mm beneath active region photospheres (Lindsey and Braun, 1998b; Lindsey and Braun, 1999), ‘acoustic glories’ surrounding complex active regions (Braun and Lindsey, 1999) and the first helioseismic images of a solar flare (Donea, Braun, and Lindsey, 1999). Phase-sensitive holography confirms the presence of reduced sound travel-time

<sup>\*</sup>Visitor, Joint Institute for Laboratory Astrophysics, University of Colorado, Boulder, CO 80309-0440, U.S.A.

<sup>†</sup>Current mailing address: Colorado Research Associates, 3380 Mitchell Lane, Boulder, CO 80301, U.S.A.



perturbations in sunspots, and has now clearly discriminated and quantified similar perturbations in acoustic moats and isolated plages. These may explain the solar cycle dependence of global  $p$  modes (Braun and Lindsey, 2000b). Holographic phase diagnostics have also led to the discovery that magnetic regions significantly reflect  $p$  modes above the acoustic cut-off frequency, where the surface of the quiet Sun acts as a nearly perfect absorber of incident acoustic radiation (Braun and Lindsey, 2000a) (see Figure 6). A review of the scientific accomplishments of helioseismic holography is given elsewhere in this volume (Braun and Lindsey, 2000a).

The basic principle of helioseismic holography is the phase-coherent computational reconstruction of the acoustic field into the solar interior, or even possibly the far side of the Sun, based on seismic disturbances observed on the near surface, so as to render stigmatic images of subsurface sources that give rise to these disturbances. This is very much how the eye treats the electromagnetic field at the surface of the cornea to secure diagnostics into the outlying world. The term ‘holography’ derives from the strong analogy to the electromagnetic holography conceived by Dennis Gabor in the late 1940s, and developed in the 1960s by E. Leith and J. Upatnieks using lasers, to render 3-dimensional optical images by the phase-coherent reconstruction of monochromatic radiation recorded on photographic ‘holograms’. The analogy to solar seismic holography is clear once the reader sees past the clever, but somewhat cumbersome, contrivances based on interference devised to register phase information onto photographic plates. These schemes generally require radiation with macroscopic coherence lengths. Holographic reconstruction employing lasers is thus nominally monochromatic, an encumbrance that does not apply to computational seismic holography.

The basic concept of helioseismic holography was first proposed by Roddier, (1975). The concept was re-introduced and extensively developed over the 1990s by Lindsey and Braun (1990), Braun *et al.* (1992), Lindsey *et al.* (1996), and Lindsey and Braun (1997), in what they promoted as a crucial diagnostic to ‘local helioseismology’ in the SOHO-GONG era. In their opinion, this concept was the key to the prospect of locating and examining fine structure as deep beneath the solar photosphere as wave-mechanically possible.

It is important to distinguish seismic holography from the popular concept of tomography. The tomography that is so powerful in X-ray medical applications suffers from poor statistics combined with severe diffraction effects that significantly impair spatial resolution when applied to the solar acoustic spectrum. Solar acoustic holography specifically proposes to address these difficulties. Seismic holography should *not* be identified as a method for physical *modelling* of solar interior structure. While holographic imaging offers a firm basis for powerful local interior modelling techniques, holographic images cannot be treated as actual physical models of solar interior anomalies themselves in any practical capacity.

The diagnostic that Chang *et al.* (1997) applied to observations from the Taiwan Oscillations Network (TON), presenting it under the name ‘ambient acoustic

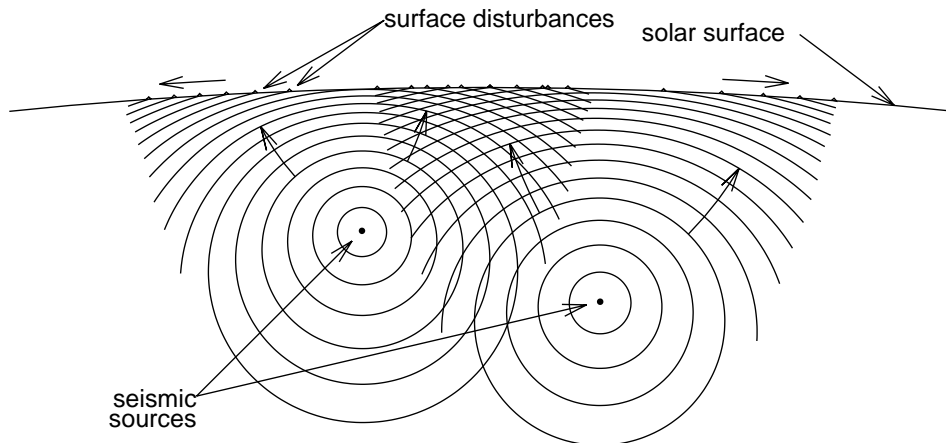
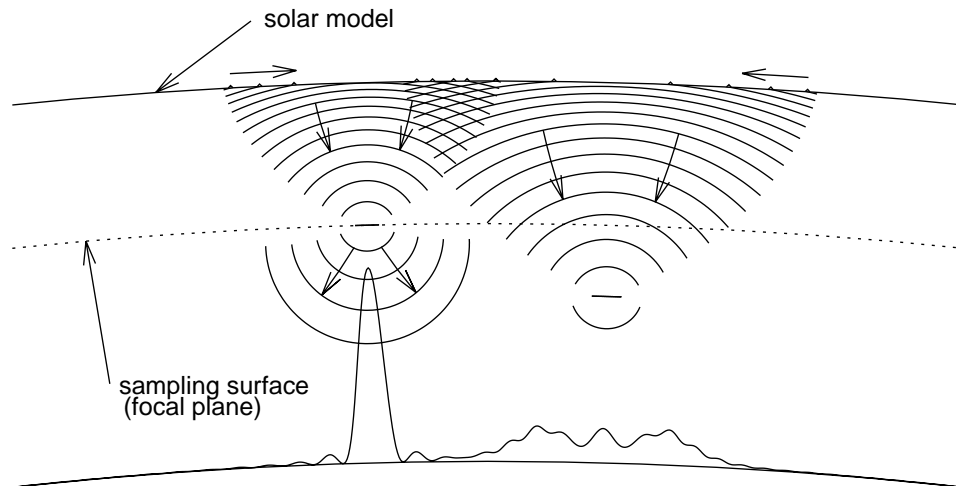


Figure 1. Seismic waves emanating from submerged sources produce surface disturbances that propagate symmetrically outward from points directly above, as indicated by arrows.

imaging' and in subsequent publications (Chen *et al.*, 1998; Chou *et al.*, 1999) as 'acoustic imaging', is quite literally helioseismic holography. Lindsey and Braun (1990) and Braun *et al.* (1992) define helioseismic holography specifically in terms of 'seismic imaging' by phase-coherent reconstruction of the acoustic field into the solar interior. They apply the terms 'seismic imaging' and 'helioseismic imaging' in a broader context that include partially coherent acoustic signatures that Lindsey and Braun (1990) suggested would appear at the antipodes of far-side acoustic absorbers. The subject of this review is specifically *holographic* seismic imaging, a generality that we mean to apply to the far surface of the Sun, to the near surface and subsurface, and to the deep interior alike.

## 2. Basic Principles of Computational Seismic Holography

The major general advantage which local helioseismology offers to solar interior diagnostics seems to be the strong parallel of wave mechanics in the solar seismic domain to electromagnetic optics. The application of holography in the solar seismic context is best illustrated with a simple example. We will consider the idealized case of a solar interior that contains a few well defined acoustic sources (Figure 1). These sources emit a pattern of waves that to some degree fills the entire solar interior, but the only part of this which we observe is a pattern of surface ripples that propagate concentrically outward (see arrows above surface) from points on the surface directly above their respective sources. For simplicity, we suppose that the waves that produce these ripples are absorbed upon their first encounter with the surface, an assumption that is generally quite accurate for frequencies above  $\sim 5.5$  mHz.



*Figure 2.* Holographic regression of the surface acoustic field into the solar interior. Surface disturbances in the neighborhood overlying submerged sources are applied in time reverse to a sourceless acoustic model of the solar interior and computationally propagated back into the model interior. The underlying acoustic field differs in important respects from that actually produced by the sources. Nevertheless, a well-appropriated sampling of the regressed acoustic field renders localized sources with strong, compact signatures at appropriate depths. The seismic signature of a source that lies considerably below or above the sampling surface is rendered by a signature that is substantial but significantly out of focus.

The basic diagnostic exercise of seismic holography, then, is to apply the seismic observations of the solar surface in time reverse to a computational solar acoustic model devoid of sources, sinks, or scatterers. This is illustrated in Figure 2. In general, we do this over a limited part of the solar surface. Borrowing from standard optical terminology, we call the region over which we apply the observed disturbance to the model the ‘pupil’ of the computation. Given appropriate computational rules, the now incoming ripples drive appropriately ingoing waves that converge back towards the locations of the sources. This acoustic regression is implemented over some extended volume and can be sampled over arbitrary surfaces. If we sample the acoustic power in a surface, i.e., a ‘focal plane’, at the depth of a source, the result should be a diffraction-limited signature such as that which appears beneath the location of the source to the left in Figure 2. If the focal plane is moved above or below the source, the signature does not generally disappear but rather defocuses, rendering a diffuse profile like that beneath the source to the right in Figure 2.

Figure 3 illustrates the 3-dimensional perspective which holographic reconstruction presents to the analyst who views the regressed acoustic signatures. In this simulation, random acoustic noise has been introduced into a solar acoustic model that contains alphanumeric absorbers just beneath the surface and at a depth of 56 Mm. As the focal plane submerges beneath the absorber, the sharp silhouette

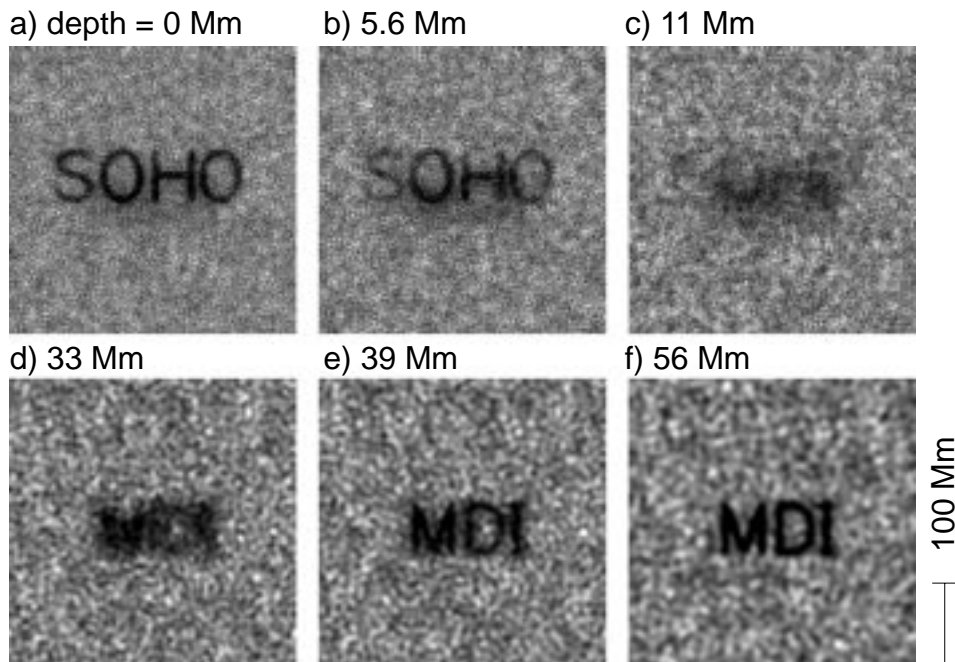


*Figure 3.* Holographic images of artificial seismic noise that encounters alphanumeric absorbers just beneath the surface and at a depth of 56 Mm. In this model, the absorbers are confined to infinitely thin sheets. Submergence of the focal plane beneath an absorber results not in its disappearance but rather a defocusing of the signature. Diffuse ‘acoustic stalactites’ extending directly beneath all surface features are an expected artifact, and not generally the signature of a significant acoustic perturbation substantially beneath the absorber.

of the absorber does not simply disappear but rather defocuses to a diffuse blur. We call this underlying plume the ‘acoustic stalactite’ of the absorber. As the focal plane approaches the depth of the deep absorber, a diffuse ‘acoustic stalagmite’ first appears, which sharpens to a diffraction-limited silhouette of that absorber when the focal plane arrives at 56 Mm. Acoustic stalactites and stalagmites are the reason the images themselves are inappropriate as models of the absorbers that produce the signatures. In the presentation illustrated in Figure 3, depth diagnostics must be accomplished by focus/defocus rather than the appearance/disappearance that would characterize the sampling of a realistic physical model of the absorber that gives rise to the signature.

Seismic holography is *not* in any sense a representation or approximation of solar acoustics in terms of ray optics. The computational regression illustrated by Figure 3 is a fully wave-mechanical one incorporating all of the effects of interference and diffraction, just as these apply to standard electromagnetic holography and lens optics. As such, seismic holography is subject to the same fundamental limitations in terms of diffraction and statistics as any other diagnostic based on helioseismic observations. It is likewise open to the full range of standard opti-

cal techniques that have been developed to optimize the informational content of coherent electromagnetic radiation.

### 3. The Computational Task

The numerical calculations for holographic extrapolation to subsurface layers can be approached in different ways. Lindsey and Braun (1997) recognize two general perspectives: (1) the ‘spectral,’ which represents the disturbance in terms of the normal modes of the medium, and (2) the ‘time-distance,’ which is closer to that of the time-distance helioseismology of Duvall *et al.* (1993). Practicality has since imposed the need for a more flexible language. We now employ the terms ‘space-time,’ and ‘wavenumber-frequency,’ and combinations thereof to discuss the computational practicalities of holography. It is the space-time perspective that is the most amenable to intuition. We will therefore proceed to present the basic practicalities of computational holography in this language.

In principle, if we are given both the acoustic amplitude and its derivative normal to any closed surface surrounding a medium free of sources, sinks and scatterers, then we can extrapolate the acoustic field anywhere in the interior of the surface, by standard Kirchhoff integral theory (see Born and Wolf, 1975a, for a presentation of the Kirchhoff integral theory for a uniform medium). In practice, helioseismic observations are much less complete than this. The ‘reconstruction’ which we derive by applying the Kirchhoff integral to incomplete data over a limited fraction of the solar surface can be regarded as a significant component of the underlying acoustic field but not by any means the actual acoustic field, even for a medium devoid of physical anomalies. From this point, we will therefore distinguish between our incomplete regression,  $H$ , of the acoustic field, and the acoustic field itself,  $\psi$ .

In the space-time perspective, the regression of the acoustic field,  $\psi(\mathbf{r}', t')$ , from the surface, where it is secured at time  $t'$  and horizontal location  $\mathbf{r}'$ , to a depth  $z$ , directly beneath horizontal location  $\mathbf{r}$  at time  $t$ , is expressed by a formalism which Lindsey and Braun (1997) call the ‘acoustic egression’. The acoustic egression,  $H_+(\mathbf{r}, z, t)$ , is an incomplete but coherent assessment of the local acoustic disturbance that has emanated from the ‘focal point,’  $(\mathbf{r}, z)$ , of the computation at time  $t$  based on its succeeding emergence at the overlying solar surface, over the range of locations and times expressed by  $(\mathbf{r}', 0, t')$ . This can be represented by an integral of the form

$$H_+(\mathbf{r}, z, t) = \int dt' \int_{a < |\mathbf{r} - \mathbf{r}'| < b} d^2\mathbf{r}' G_+(|\mathbf{r} - \mathbf{r}'|, z, t - t') \psi(\mathbf{r}', t'). \quad (1)$$

Here  $G_+$  is a Green’s function that expresses how a single transient point disturbance at  $(\mathbf{r}', 0, t')$  propagates backwards in time to  $(\mathbf{r}, z, t)$ . It equivalently ex-

presses how a single transient point disturbance at  $(\mathbf{r}, z, t)$  propagates forwards in time to arrive at  $(\mathbf{r}', 0, t')$ .

The ‘acoustic *ingression*’,  $H_-$ , is the time reverse of the *egression*  $H_+$ . It rather expresses waves coherently converging *into* the focal point,  $(\mathbf{r}, z)$ , to contribute to the disturbance, rather than emerging *from* the disturbance. The *ingression* is computed simply by replacing the Green’s function,  $G_+$ , in Equation (1) by its time reverse,

$$G_-(|\mathbf{r} - \mathbf{r}'|, z, t - t') = G_+(|\mathbf{r} - \mathbf{r}'|, z, t' - t) . \quad (2)$$

In our applications, the pupil of the computation is generally an annulus surrounding the focal point,  $\mathbf{r}$ , whose inner radius is  $a$  and outer radius is  $b$ , or a disk, in which case  $a = 0$ .

Once the task of computing the *egression*,  $H_+$ , is accomplished over an appropriate region, under an appropriate pupil, over a sufficient range in time,  $t$ , it can simply be squared and integrated over any desired portion of that range in time to yield an *egression* power map over that time interval. The first applications of seismic holography, to observations from the Taiwan Oscillations Network (Chang *et al.*, 1997), confirmed the well known  $p$ -mode absorption in sunspots discovered earlier from Hankel analysis (Braun, Duvall, and LaBonte, 1988). A remarkable array of discoveries proceeded from the application of the diagnostic to SOHO-MDI observations. These include ‘acoustic moats’ surrounding sunspots (Braun *et al.*, 1998; Lindsey and Braun, 1998a), acoustic glories marking the quiet outer fringes of complex active regions (Braun and Lindsey, 1999) and apparent ‘acoustic condensations’ 10–20 Mm beneath the photosphere. We refer to Braun and Lindsey (2000a) for a review.

The computational advantage of the wavenumber-frequency perspective over the space-time is a result of the temporal and horizontal spatial invariance of the Green’s function,  $G_+$ . For a plane parallel atmosphere, the normal modes are functions whose projections at the surface (or any horizontal plane) are simple running plane waves, for which convolution reduces to a simple product. If  $\hat{\psi}(\mathbf{k}, \nu)$  represents the Fourier transform of  $\psi(\mathbf{r}, t)$  with respect to  $\mathbf{r}$  and  $t$ , and  $\hat{G}_+(|\mathbf{k}|, z, \nu)$  represents the same of  $G_+(|\mathbf{r}|, z, t)$  truncated by the pupil, then the convolution theorem reduces Equation (1) to the product

$$\hat{H}_+(\mathbf{k}, z, \nu) = \hat{G}_+(|\mathbf{k}|, z, \nu), \hat{\psi}(\mathbf{k}, \nu) , \quad (3)$$

where  $\hat{H}_+(\mathbf{k}, z, \nu)$  is the Fourier transform of the *egression*. The *egression* can thus be computed very rapidly, using the fast Fourier transform to shift expediently between the wavenumber/frequency to the space/time perspectives as needed. All of the examples that appear in this paper and those that are reviewed by Braun and Lindsey (2000a) were computed in the wavenumber-frequency perspective for this reason.

The plane parallel projection of the Sun’s spherical surface in the foregoing formalism introduces optical aberrations into the computation. These aberrations

are modest for small pupils and have their practical analog in the familiar Seidel aberrations of standard electromagnetic optics. The analogs of spherical aberration, distortion, and curvature of field are easily corrected (Braun *et al.*, 1998). However, coma, primary astigmatism and higher-order aberrations cannot be avoided for the large pupils that are needed to image deep focal planes or the far-side of the Sun, and this eventually prevents stigmatic imaging substantially away from the center of the projection under the plane-parallel approximation. The transform to wavenumber perspective must then be abandoned.

If we let  $\check{\psi}(\mathbf{r}, \nu)$ ,  $\check{H}_{\pm}(\mathbf{r}, z, \nu)$ , and  $\check{G}_{\pm}(|\mathbf{r}|, z, \nu)$  be just the temporal Fourier transforms of  $\psi(\mathbf{r}, t)$ ,  $H_{\pm}(\mathbf{r}, z, t)$ , and  $G_{\pm}(|\mathbf{r}|, z, t)$ , respectively, then the egression computation reduces to

$$\check{H}_{+}(\mathbf{r}, z, \nu) = \int_{a < |\mathbf{r} - \mathbf{r}'| < b} d^2\mathbf{r}' \check{G}_{+}(|\mathbf{r} - \mathbf{r}'|, z, \nu) \check{\psi}(\mathbf{r}', \nu), \quad (4)$$

where  $\mathbf{r}$  and  $\mathbf{r}'$  indicate locations on the Sun's spherical surface. We do not presently know of a palatable way to avoid the integral over both spatial dimensions when the plane-parallel projection is not appropriate. However, the need for a large pupil is generally commensurate with a spatial spectrum that is restricted to a relatively compact range in spherical harmonic degree,  $\ell$ , which is amenable to a proportionately coarser sampling both of the pupil and the image field. This requires only that the data are first appropriately smoothed to prevent aliasing. The computational load imposed by this task can therefore be considerably alleviated.

#### 4. Subjacent Vantage Holography

In the conceptual examples illustrated by Figures 1 and 2, we considered radiation that had emanated upward from a submerged source to arrive at the overlying surface more or less directly. This is what we call 'superjacent vantage holography'. However, if we fashion the pupil of the computation to be an annulus whose inner radius is much greater than the depth of the focal plane, then the optical paths that connect the source to the pupil represent radiation that initially emanated downward, penetrating deep beneath the solar surface before refracting back to the reach the surface at the pupil a considerable distance away. We call this 'subjacent vantage holography'. This geometry is illustrated in Figure 4. Subjacent-vantage holography is quite often the practical choice, since the superjacent signature directly above a shallow source of interest typically appears in an attendant active region whose photosphere introduces phase and amplitude perturbations that offer confusion. By extending the pupil to a relatively quiet photosphere clear of the active region, the analyst effectively renders the source from the perspective of a submerged acoustic observer looking upward into the bottom of the acoustic source along optical paths that circumvent the overlying surface activity.

An important consideration regarding subjacent vantage holography where diffraction is concerned is that the relation of the pupil to the illuminating cone is

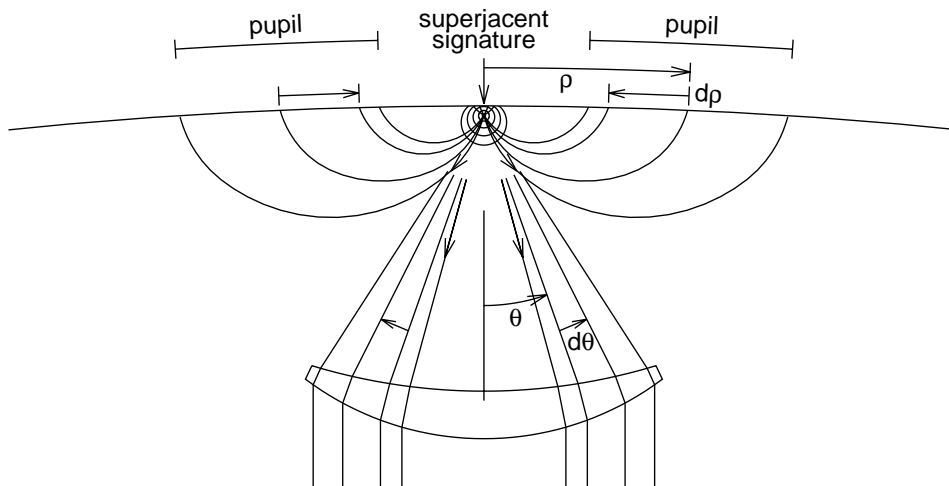


Figure 4. Subjacent vantage imaging is the result of a holographic regression in which the focal plane is shallow compared to the inner radius of the pupil. This configuration images seismic radiation that is initially emitted downward from the source and penetrates thousands of km into the solar interior before being refracted back to the surface. While the acoustic disturbance is necessarily observed at the surface, these images render the perspective of an acoustic observer looking upward into the base of the source from thousands of km beneath it. In subjacent vantage holography, the disposition of the computational pupil is substantially an inversion of that in familiar lens optics. As the angle,  $\theta$ , of illumination at the focal point increases, the angular distance,  $\rho$ , along the pupil from its center, above the focal point, decreases.

*inverted* with respect to that of familiar lens optics. In familiar lens optics, the greatest angle of illumination,  $\theta$ , corresponds to the periphery of the aperture. In this case, and in superjacent-vantage holography of deeply submerged sources, the resolution limit imposed by diffraction is optimized by using a larger pupil. In subjacent vantage holography, it is the *inner* radius of the pupil that is connected to the optical path of the greatest illuminating angle. The diffraction limit is, therefore, set not by how wide the outer radius of the pupil is but rather how *compact* the *inner* radius is. This principle may come across more intuitively to some readers in more strictly wave-mechanical language. For this purpose we point out that the finest diffraction limit for the computation is accomplished by securing the waves with the highest spherical harmonic degree,  $\ell$ . In the subjacent vantage, these are the waves with the shortest skip distances from the source. These are therefore the waves that arrive more towards the inside of the pupil, not the outside as the high- $\ell$  waves do in familiar lens optics.

The simulations shown in Figure 3 were made with a annular pupil with inner radius,  $a = 15$  Mm and outer radius  $b = 45$  Mm. The signatures shown in the first two frames, a and b, are entirely from a subjacent perspective and the third from a mixed perspective that is predominantly subjacent. The deeper alphanumeric absorber is seen from perspectives that are predominantly superjacent.

### 5. An Example

Figure 5, adapted from Lindsey and Braun (1998b), shows the formalism described above applied to NOAA AR 7973, a single isolated sunspot, integrated over a 24-hr interval beginning on 25.0 June 1996. The left column shows egression power maps of the region in a 1 mHz passband centered at 6 mHz. Focal-plane depths are indicated to the left of respective frames in the left column by numerical values, and graphically with vertical bars, by their respective vertical dimensions. The right column shows comparative egression power signatures of localized superficial absorbers in a plane parallel acoustic model illuminated by a random, isotropic noise spectrum. The superficial absorbers, represented by Rorschach splotches in the upper-right frame, were intended for comparison between egression power maps at depth zero of the active region and the model. The pupil for these computations is an annulus extending from inner radius  $a = 15$  Mm to outer radius  $b = 45$  Mm (identical to that used in the computations that produced Figure 3). This annulus is shown in the upper right frame centered on the Rorschach splotch to the right of frame center.

The model signatures (right column) provide a gauge of the acoustic stalactites that appear beneath superficial absorbers, and thereby an assessment of the sensitivity of focus with respect to depth. These suggest that the egression signature of the sunspot umbra is roughly consistent with absorption that is entirely superficial. A conspicuous satellite appearing north-east of the umbral signature is indicated in the left column by arrows. This signature persists to 11.2 Mm, at which depth the stalactite attached to its superficial counterpart in the model has essentially disappeared.

Acoustic contrasts of the sunspot against its immediate surrounding were computed by comparing the egression power averaged over a small disk (radius 8.4 Mm) and the west side of a surrounding annulus, to avoid the satellite. This is plotted in the lower left box of Figure 5. A similar contrast is computed for the satellite (radius 8.4 Mm) and plotted at lower right. The tendency for the contrast of a very compact superficial absorber to become negative as the focal plane submerges is quite real, a result of diffraction effects on which we will not elaborate here.

It should be clearly understood that the egression power maps in Figure 5, and those of similar depth in Figure 3, show the focal plane from a predominantly *subadjacent* perspective. The egression power image at zero depth, for example, is an image of the surface through the surrounding solar interior and should not be confused with a simple acoustic power map of the local wave amplitude as directly observed at its surface location. Each pixel in the egression-power image is a coherent representation of waves that have traveled thousands of km from that pixel, and deep beneath the solar surface, to re-emerge into an annular pupil 15–45 Mm from the pixel. The sunspot is therefore quite literally viewed through the solar interior as from beneath, not through the photosphere overlying the sunspot.

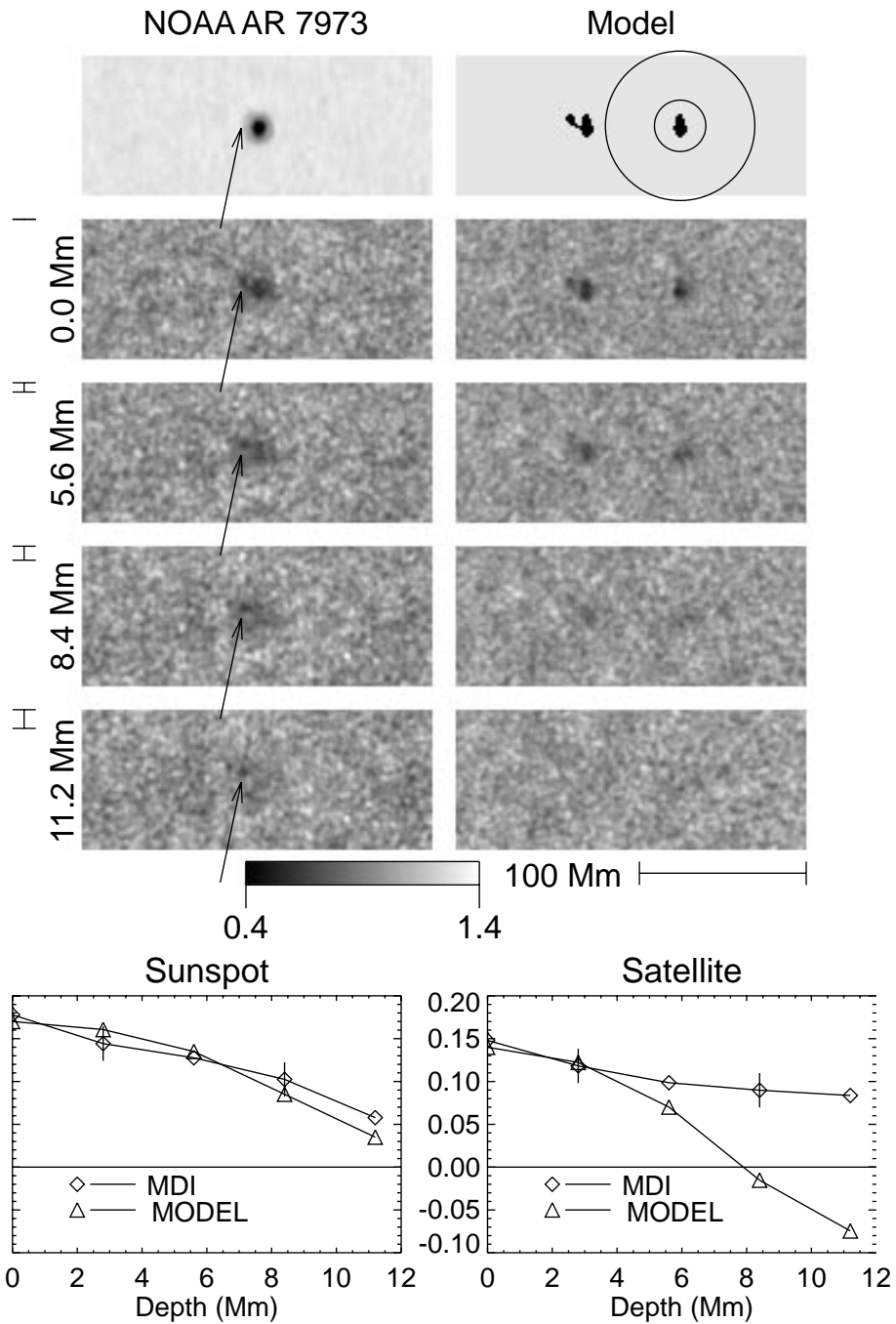


Figure 5. Egression power maps (left column) of NOAA AR 7973 integrated over 24 hr beginning at 25.0 June 1996 in 6 mHz acoustic radiation (1 mHz bandwidth). The right column shows respective egression power maps of acoustic noise propagated by a Christensen-Dalgaard model locally depleted by superficial absorbers intended to match the primary signature in the upper left egression map. The greyscale applies to the egression power, normalized to unity for the quiet Sun. Arrows in the left column locate a satellite of the primary acoustic deficit signature. Focal-plane depths are indicated to the left of respective frames by numerical values and by vertical bars. The computational pupil is indicated by the annulus drawn in the upper right frame. Sunspot and satellite contrasts are plotted in the lower left and right boxes, respectively.

An unfortunate optical consequence of the increase in sound speed with depth in the solar interior is an increasing wavelength and hence a coarser diffraction limit at the greater depths for any given frequency. The effects of this are evident in a serially deteriorating resolution of the images shown by Figures 3(d–f) as the focal plane submerges. This illustrates a fundamental limitation that applies to holography on the same terms as for all other helioseismic diagnostics.

## 6. Acoustic Modelling Based on Holographic Images

Comparisons with simple models such as those shown above encourage the prospect of flexible procedures, including inversions, that would characterize the acoustic environment in physical terms such as acoustic emissivity and opacity, and refractivity and flow velocity when phase-sensitive holography is applied.

Inversions can probably be addressed from a broad variety of independent avenues. Where the Born approximation applies in zeroth or first order, for example, holographic images of a source,  $S(\mathbf{r}', z')$ , distributed over a domain of horizontal location  $\mathbf{r}'$  and depth,  $z'$ , can be represented by a Fredholm integral of the form

$$\langle |H_+(\mathbf{r}, z)|^2 \rangle = \int d^2\mathbf{r}' \int dz' \mathcal{G}(|\mathbf{r} - \mathbf{r}'|, z, z') S(\mathbf{r}', z'), \quad (5)$$

where the angular brackets indicate statistical averaging over appropriate intervals in time and frequency. Here,  $\mathcal{G}$  is a Green's function representing the egression-power signature of a point emitter of unit acoustic luminosity at  $(\mathbf{r}', z')$ . To the extent that the egression power signature renders a point source quite sharply in focal planes at the depth of the source,  $z = z'$ , the Green's function,  $\mathcal{G}(|\mathbf{r} - \mathbf{r}'|, z, z')$ , can be substantially inverted in practical terms. Broadly speaking, there exists a fairly straight-forward class of functions,  $\mathcal{G}^{-1}(|\mathbf{r} - \mathbf{r}'|, z, z')$ , such that the integral

$$S(\mathbf{r}, z) = \int d^2\mathbf{r}' \int dz' \mathcal{G}^{-1}(|\mathbf{r} - \mathbf{r}'|, z, z') \langle |H_+(\mathbf{r}', z')|^2 \rangle \quad (6)$$

will generally represent the source distribution faithfully, within resolution limits consistent with the acuity of  $\mathcal{G}$  in the neighborhood of  $(\mathbf{r}', z')$ . The more complex inversion problems that involve absorbers require the extension of the Born approximation to higher orders and, in the case of scatterers, the incorporation of phase-sensitive diagnostics into the formalism.

## 7. Phase-Sensitive Holography

The purpose of phase-sensitive holography in the solar acoustic context is to incorporate the basic utilities of optical interferometry into solar interior diagnostics. Phase-sensitive seismic holography finds strong analogies in the phase-contrast

imaging of Zernike (see Born and Wolf, 1975b), Schlieren imaging (Born and Wolf, 1975c) and Michelson interferometry (Born and Wolf, 1975d) in familiar electromagnetic optics. The concept is expressed most simply in the space-frequency perspective, but its strongest analogy in helioseismic research to date is in the measurement of time-distance correlations as developed by Duvall *et al.* (1993). The general concept of seismic holography predates that of ‘time-distance helioseismology’ by several years. However, the phase-sensitive diagnostics which Lindsey and Braun (1997) developed for solar acoustic holography can be regarded as a direct incorporation of the time-distance correlations of Duvall *et al.* (1993) into the formalism of seismic holography.

The need for phase-sensitive holography is at least two-fold. It offers us a straight-forward quantitative probe of refractive anomalies such as we expect from thermal perturbations and independently of Doppler effects due to submerged flows. However, it should be kept in mind that local anomalies such as these, illuminated by isotropic acoustic noise, would be altogether undetectable without phase-sensitive diagnostics. The standard acoustic-power holography we have reviewed up to now depends for its operation on the existence of anomalous sources and absorbers. It can even detect refractors and flows by their scattering of an acoustic anisotropy created by a nearby absorber or an anomalous emitter. However, isotropically illuminated scatterers simply replace the acoustic radiation they block with radiation which they scatter from some other direction, and therefore render themselves invisible by lack of contrast with respect to the isotropic background.

Phase-sensitive holography can be visualized in terms of a gedanken experiment in which we contrive to focus monochromatic acoustic radiation, of frequency  $\nu$ , into a refractive sample, as illustrated in Figure 6, by driving the solar surface on the right side of the sample so as to produce waves that converge into it accordingly. If the sample is refractively similar to that of the ambient medium, the waves should pass through it with neither a delay nor an advancement. In that case, a computation of the egression in the pupil covered by the outgoing waves to the left of the sample will be equal to the ingression from the pupil on the right, and the phase shift between the two will be null. However, if the sample contains a refractive perturbation,  $\Delta n = \Delta c/c$ , where  $c$  is the nominal speed of sound in the neighborhood of the sample, then the transit of the wave through the sample should be delayed by a time

$$\Delta t \sim a \Delta n/c, \quad (7)$$

where  $a$  is the characteristic diameter of the sample. The phase,  $\phi$ , is accordingly delayed by

$$\Delta\phi \sim 2\pi\nu a \Delta n/c, \quad (8)$$

To relate  $\Delta\phi$  to  $H_+$  and  $H_-$ , we define the temporal Fourier transforms,  $\check{H}_+$  ( $\mathbf{r}, z, \nu$ ) and  $\check{H}_-$  ( $\mathbf{r}, z, \nu$ ) of  $H_+(\mathbf{r}, z, t)$  and  $H_-(\mathbf{r}, z, t)$ , respectively. Then,

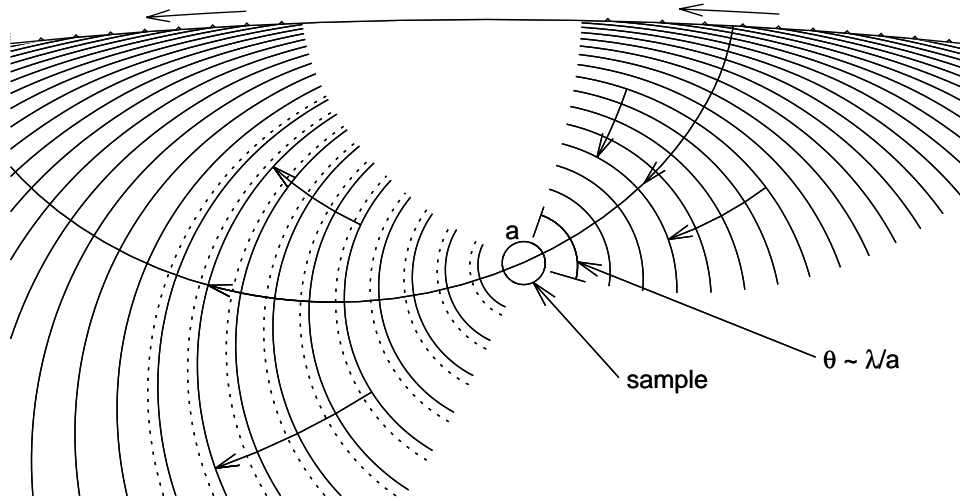


Figure 6. Solar acoustic holography recognizes that the optimal illumination of a sample is secured not by random noise or by seismic radiation from a distant point source but rather by a pattern of seismic radiation that is *focused* directly into the sample over a range of illuminating angles that securely encompasses the diffraction limit,  $\theta = \lambda/a$ . If this is accomplished, by appropriately driving a sufficiently extensive region of the solar surface, then it is possible to extrude most of the acoustic power through a sample that is little more than a wavelength in diameter. In that case, the phase delay of the radiation emerging from the sample will be represented by a value of order  $2\pi a \Delta n/c$ , where  $a$  is the characteristic path length through the sample.

$$\Delta\phi = \arg(\langle \check{H}_+(\mathbf{r}, z, \nu) \check{H}_-^*(\mathbf{r}, z, \nu) \rangle_{\Delta\nu}), \quad (9)$$

where the angular brackets indicate an average over bandwidth  $\Delta\nu$  in frequency that must be sufficient for the statistical requirements that apply. The equivalent diagnostic in the temporal domain is derived from the temporal correlation,

$$C(\mathbf{r}, z, \tau) = \int dt' H_-(z, \mathbf{r}, t') H_+(z, \mathbf{r}, t' + \tau). \quad (10)$$

A localized refractive perturbation,  $\Delta n$ , almost anywhere in the medium will generally have a minimal effect on this correlation. However, such a perturbation centered at a mutual focal point,  $(\mathbf{r}, z)$ , of  $H_+$  and  $H_-$  can be expected to shift the temporal peak of the correlation from  $\tau = 0$  to a value  $\Delta t$  of the order expressed by Equation (7).

Applications of this diagnostic by Braun and Lindsey (2000b) clearly render sunspots with travel time reductions of order 40 s, plages with reductions ranging up to 15 s and acoustic moats with reductions in the range 4–5 s. These perturbations are of roughly sufficient order to explain frequency shifts of low- $\ell$  modes with the solar cycle (see Jiménez-Reyes *et al.*, 1998).

Lindsey and Braun (1997) propose an extension of the correlation expressed by Equation (10) for the purpose of measuring horizontal flows. This is based on the

concept that a sample moving at velocity  $\mathbf{v}$  will displace the waves passing through it a distance  $\Delta \mathbf{r} = \mathbf{v} \Delta t$  during their transit and therefore physically displace the attendant egression,  $H_+$ , with respect to the ingression,  $H_-$ . Accordingly, they define the correlation

$$C(\mathbf{r}, z, \mathbf{s}, \tau) = \int dt' H_-(z, \mathbf{r}, t') H_+(z, \mathbf{r} + \mathbf{s}, t' + \tau), \quad (11)$$

whose nominal peak in a stationary medium should be spatially located at  $\mathbf{s} = \mathbf{0}$ . The effect expected of the flow is to displace the correlation peak spatially by a distance of order

$$\Delta \mathbf{r} = \mathbf{v} \Delta t = \mathbf{v} a \Delta n / c. \quad (12)$$

Without further elaboration we note that, in the space-frequency perspective, the Doppler information contained in Equation (11) can be derived from the complex vector correlation

$$\mathbf{U}(\mathbf{r}, z) = \langle \check{H}_-^*(\mathbf{r}, z, \nu) \nabla \check{H}_+(\mathbf{r}, z, \nu) \rangle_{\Delta \nu}. \quad (13)$$

Preliminary uncalibrated experiments with this diagnostic by Braun and Lindsey (2000a) (see Figure 10) clearly show supergranular flows, as well as significant outflows from sunspots.

## 8. Green's Functions

The Green's function,  $G_{\pm}(|\mathbf{r} - \mathbf{r}'|, z, t - t')$  (see Equation (1)) characterizes the acoustics of the solar model to which helioseismic observations,  $\psi(\mathbf{r}', t')$ , are applied to accomplish acoustic regressions. Computational seismic holography is intended as a broad and flexible diagnostic generality, not to be confined to any particular model. For this purpose it is important to keep a clear distinction between the solar acoustic model and the solar interior itself. Indeed, the Green's function can deviate fairly blatantly from what we know of real solar interior acoustics and deliver remarkably high-quality and diagnostically useful images. We will proceed to outline some basic intuitive concepts that make it fairly easy to fashion Green's functions appropriate for practical diagnostic applications. It should be kept in mind that what we present here is only one of any number of suitable ways to approach this problem.

In Section 3, we used the notation  $G_+(|\mathbf{r} - \mathbf{r}'|, z, t - t')$  to indicate a Green's function that regresses a disturbance backwards in time from a location and time  $(\mathbf{r}', 0, t')$  on the solar surface to a location  $(\mathbf{r}, z, t)$  in the solar interior. Given an acoustic formalism in which the field,  $\psi$ , is appropriately normalized with respect to energy flux, and solar interior acoustics in the absence of sources and sinks is time-reversal invariant, the same Green's function also characterizes the propagation of an acoustic pulse that emanates from a unit transient source at  $(\mathbf{r}, z, t)$

forward in time to manifest a disturbance at a surface point  $(\mathbf{r}', 0, t')$ . For the following discussion this will be the interpretation, and in the future we will apply these interpretations interchangeably.

### 8.1. DISPERSIONLESS ACOUSTICS

To begin with, we consider the general problem of acoustics in an atmosphere with no dispersion. In such a model, a transient pulse, emitted at depth  $z$  beneath surface location  $\mathbf{r}$  at time  $t$  propagates outward from  $(\mathbf{r}, z)$  in the form of a disturbance confined to an infinitely thin surface, a wavefront. When the wavefront passes through a distant point  $\mathbf{r}'$  at the solar surface, this location responds with a ripple characterized by the same infinitely sharp temporal profile as the source but appropriately attenuated. We will assume that this Green's function is invariant both with respect to time and to horizontal translation. It can therefore be expressed in the form

$$G_+(\mathbf{r} - \mathbf{r}', z, t - t') = \delta(t - t' - T(|\mathbf{r} - \mathbf{r}'|, z)) f(|\mathbf{r} - \mathbf{r}'|, z). \quad (14)$$

Here, the function  $T$  expresses the travel time from  $(\mathbf{r}, z)$  to  $(\mathbf{r}', 0)$ ,  $f$  expresses the amplitude of the pulse at  $(\mathbf{r}', 0)$ , and  $\delta$  represents the Dirac delta function.

The dispersionless formalism expressed by Equation (14) should not be confused with an approximation to geometrical optics. When applied to sources of finite frequency, this Green's function appropriately reproduces the effects of diffraction, just as it does in the simple case of electromagnetic optics in a vacuum. Nevertheless, standard geometrical optics does offer a simple and powerful formalism whereby to derive practical estimates of Green's functions that render diffraction-limited images when applied to holographic computations. It is important to understand that what follows is intended as a very particular model, and does not in any way consign holography itself to optics in the ray approximation, even in the narrow context of this particular example. Wave-mechanical reconstruction based on this standard eikonal formalism is the technical equivalent of using lenses designed by ray tracing to image actual radiation, which is invariably a wave.

Both  $T$  and  $f$  in Equation (14) depend critically on how the sound speed,  $c$ , varies with depth. We can derive the optimal optical path,  $\Gamma$ , satisfying Fermat's principle from Snell's law,

$$\frac{d\hat{\mathbf{t}}}{ds} = \hat{\mathbf{t}} \times (\hat{\mathbf{t}} \times \nabla \ln c), \quad (15)$$

where  $\hat{\mathbf{t}}$  is the unit tangent vector along  $\Gamma$ . Once the particular path,  $\Gamma$ , connecting  $(\mathbf{r}, z)$  to  $(\mathbf{r}', 0)$  is thus determined, the travel time,  $T$ , is obtained simply by integrating the differential travel time along  $\Gamma$ :

$$T(|\mathbf{r} - \mathbf{r}'|, z) = \int_{\Gamma} \frac{ds}{c}, \quad (16)$$

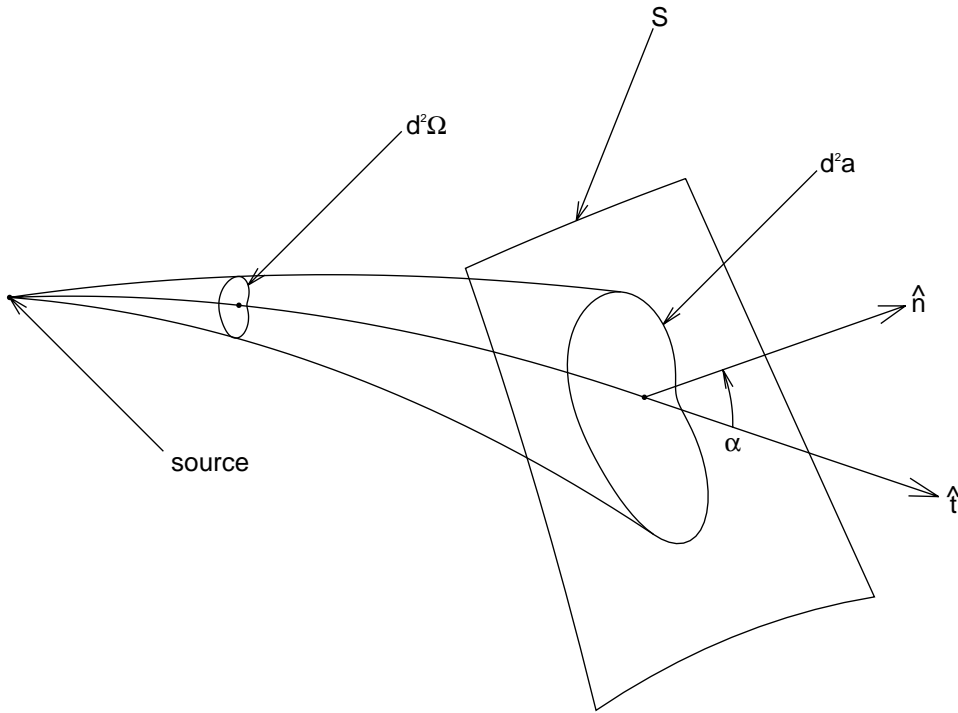


Figure 7. The intensity law of geometrical optics provides that the acoustic flux emanating from a monopolar point source, and passing through an area element  $d^2a$  on a surface surface,  $S$ , remains in proportion to the solid angle,  $d^2\Omega$ , subtended by the optical paths that envelop the boundary of  $d^2a$ .

where  $ds$  expresses the differential element of path length along  $\Gamma$ .

In the same context, the amplitude profile,  $f$ , can be derived from the intensity law of geometrical optics (Born and Wolf, 1975e). For its application to a monopolar Green's function, this simply requires that the acoustic flux emanating from a source (see Figure 7), and passing through an area element  $d^2a$  on a surface,  $S$ , must be in proportion to the solid angle,  $d^2\Omega$ , subtended by the optical paths leading to the boundary of the surface element. We represent the acoustic energy flux density by the square amplitude times the sound speed,  $cf^2$ , the unit normal to  $S$  by  $\hat{\mathbf{n}}$  and the unit tangent to the optical path, again, by  $\hat{\mathbf{t}}$ . The amplitude for an impulse of unit luminosity must then satisfy

$$cf^2 \hat{\mathbf{n}} \cdot \hat{\mathbf{t}} d^2a = \frac{d^2\Omega}{4\pi}. \quad (17)$$

For the subjacent-vantage geometry illustrated in Figure 4

$$d^2\Omega = 2\pi \sin \theta d\theta \quad (18)$$

and

$$d^2a = 2\pi \sin \rho d\rho, \quad (19)$$

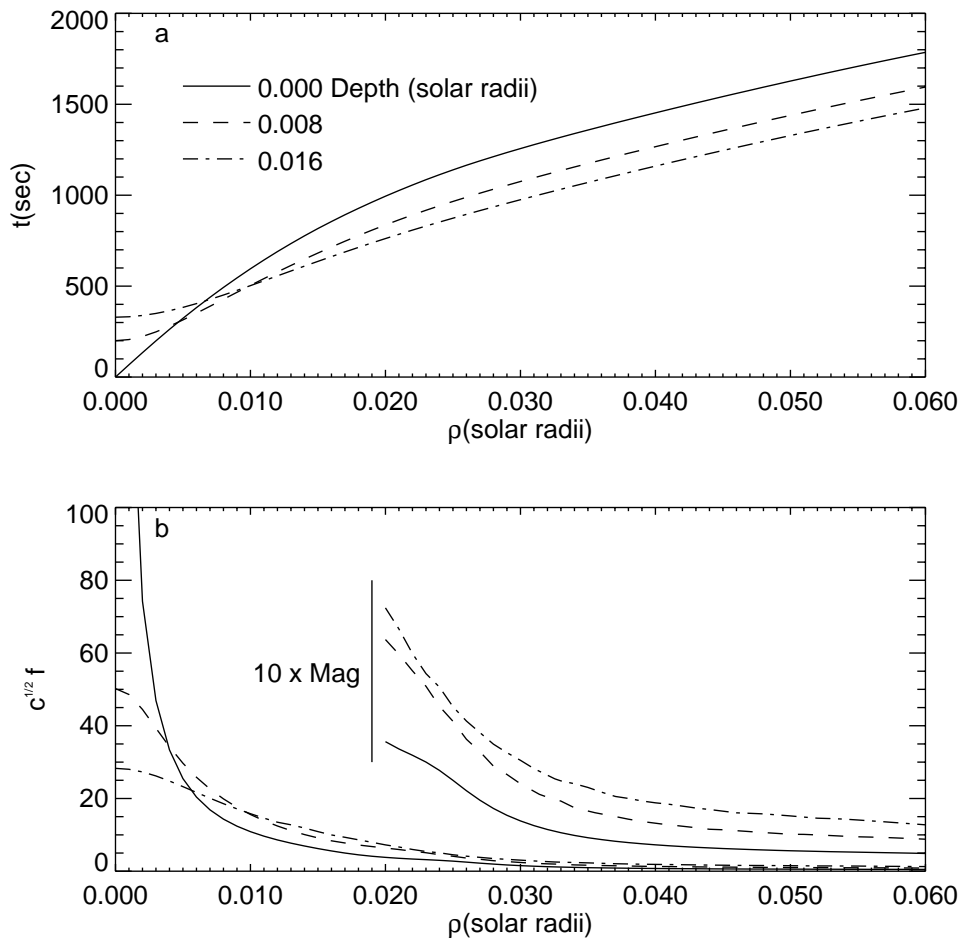


Figure 8. Plots of the single-skip travel time,  $T$  (a), and amplitude,  $f$  (b), as functions of angular distance,  $\rho$ , from the source computed for the solar model of Christensen-Dalsgaard, Proffitt, and Thompson (1993). The different curves represent various source depths as indicated in frame a. For  $\rho > 0.2$  solar radii the amplitudes are also shown multiplied by a factor of 10.

and so Equation (17) reduces to

$$f^2 = \frac{1}{4\pi c} \frac{\sin \theta}{\cos \alpha} \frac{d\theta}{\sin \rho d\rho}, \quad (20)$$

where  $\alpha$  is the angle of vertical incidence of the optical path to the surface. Figure 8 shows plots of  $T$  and  $f$  as functions of angular distance,  $\rho$ , from the source computed by the formalism above for the atmosphere of Christensen-Dalsgaard, Proffitt, and Thompson (1993).

The foregoing discussion applies to waves that are absorbed by the solar photosphere on their first encounter after leaving the source, a property that accurately characterizes waves with frequencies above 5.5 mHz. For frequencies below about

4.5 mHz the photosphere is a strong specular reflector, and the Green's function is more properly characterized by a sum of components,

$$G_+(\mathbf{r} - \mathbf{r}', z, t - t') = \sum_n \delta(t - t' - T_n(|\mathbf{r} - \mathbf{r}'|, z)) f_n(|\mathbf{r} - \mathbf{r}'|, z), \quad (21)$$

where  $n$  is an integer indexing the disturbance that has just completed its  $n$ th skip to the surface as it is being represented by the sum. The analyst is, nevertheless, free to omit any part of the Green's function and apply only that part which she prefers. She might do what we call 2-skip holography by computing the egression with only the  $n = 2$  term in the Green's function.

In multiple-skip holography imaging on significantly submerged focal planes,  $T_n$  and  $f_n$  are double valued functions of  $\rho$  outside of a well-defined minimum  $\rho$  inside of which no optical paths are allowed to arrive, geometrically. One branch consists of predominantly subjacent-vantage optical paths for which  $\rho$  decreases as the angle,  $\theta$ , of illumination increases, where  $\theta$  is measured from the reference that points vertically downward, as in Figure 4. The other branch is composed of superjacent-vantage optical paths, for which  $\rho$  increases after reaching a minimum as  $\theta$  continues to increase towards  $180^\circ$ . The two-skip profiles for  $T$  and  $f$  are plotted in Figure 9 for a source at a depth of  $0.016 R_\odot$ . The superjacent branch is indicated by solid curves and the predominantly subjacent branch by dashed curves. Optical paths from both branches conflate at  $\rho_{\min} = 0.068 R_\odot$  to form a 'caustic' similar to that which gives rise to the familiar terrestrial rainbow.

In a strict solution of the wave equation at finite frequency, the singularity at the caustic collapses to an analytic diffraction fringe. These profiles can be derived by analytical techniques based on path integrals, for example those described by Schlottman (1999). In practice, the profiles plotted in Figures 8 and 9 render high-quality, diffraction-limited seismic images, provided that the caustics are appropriately smoothed or truncated to control computational accidents otherwise admitted by the singularities. The egression power images plotted in Figures 3 and 5 were computed from the profiles plotted in Figure 8.

## 8.2. DISPERSION

The real solar interior significantly disperses acoustic waves, mainly near the surface. The dispersionless Green's function stated by Equation (14) is entirely adequate for single-skip egression power maps integrated over periods that are long compared to the range of time over which a transient source is actually dispersed upon arrival at any particular point in the pupil of the computation. However, coherent holography over more than a single skip-number (see index  $n$  in Equation (21)), phase-sensitive holography, and even single skip-number holography that proposes to resolve events over a time short compared to the temporal range of the dispersion eventually run into the need for a more realistic acoustic model than that expressed by Equation (14). The WKB approximation of standard quantum mechanics (Mes-

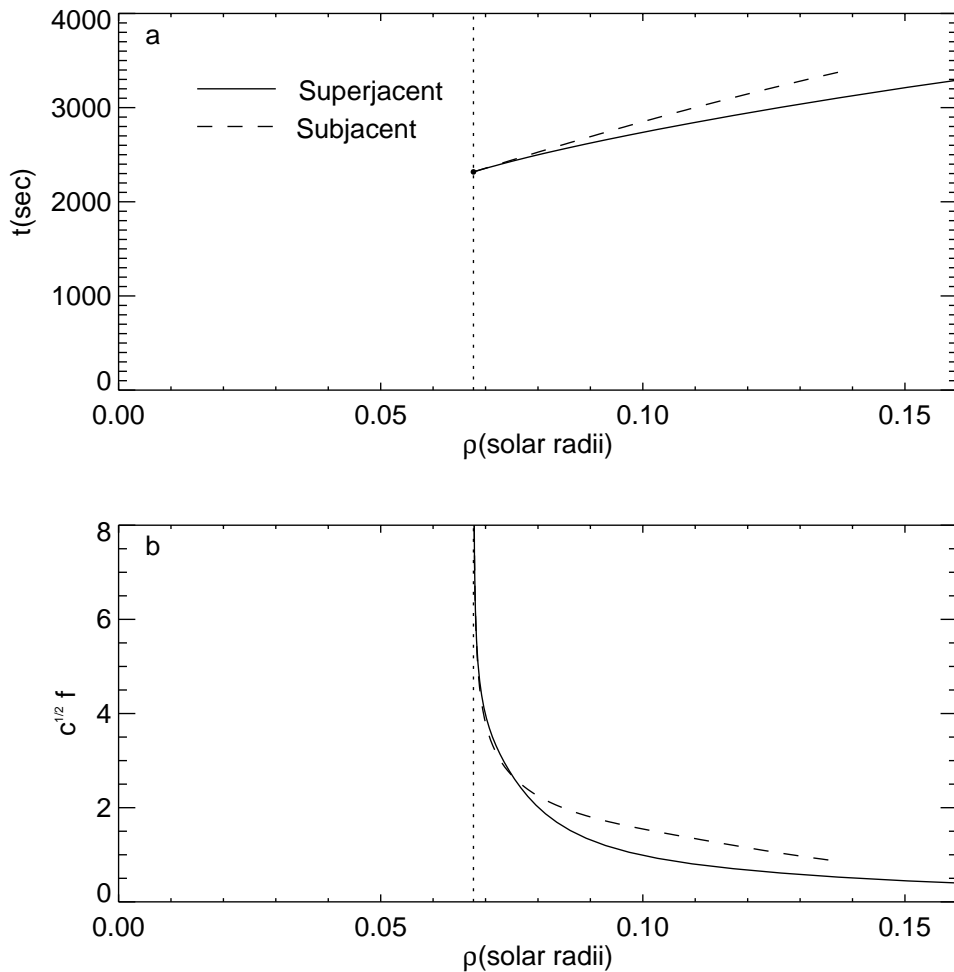


Figure 9. Plots of the two-skip travel time,  $T$  (a), and amplitude,  $f$  (b), as functions of angular distance,  $\rho$ , from the source computed by the formalism described in the text for the atmosphere of Christensen-Dalsgaard, Proffitt, and Thompson (1993). The dashed curves plot these relations for the predominantly subjacent-vantage branch of optical paths, for which the distance,  $\rho$ , from the source to the second arrival at the surface decreases with illuminating angle,  $\theta$  (see Figure 4). The solid curves plot these relations for the fully superjacent-vantage branch, for which the distance,  $\rho$ , from the source increases with  $\theta$ .

siah, 1961) offers a reliable account of dispersion for most practical purposes. We will not elaborate on this formalism here.

In the case of surface holography, dispersion can be estimated empirically over the  $p$ -mode band. Both the assessment and the correction are best made in the space-frequency perspective, that to which Equation (4) applies. The temporal Fourier transform,  $\hat{G}_{\pm}$ , of the dispersionless Green's function expressed by Equation (14) is given by

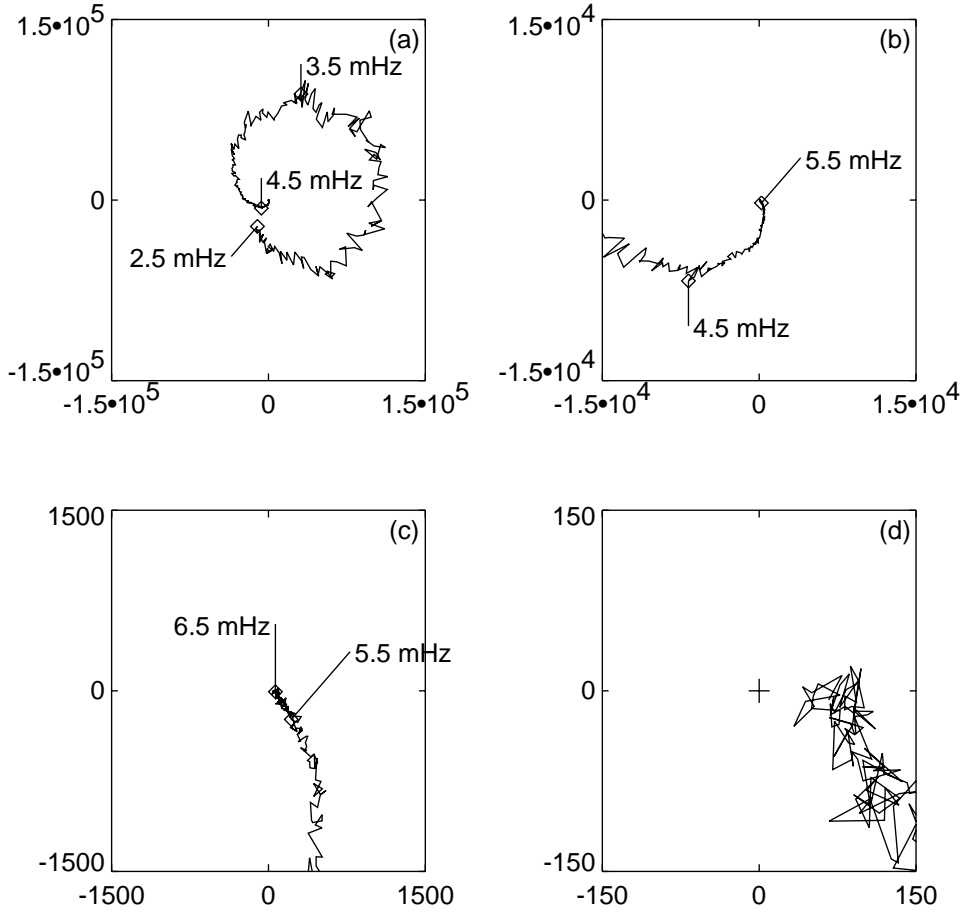


Figure 10. The phase correlation,  $\langle \hat{H}_+(\mathbf{r}, \nu) \hat{\psi}^*(\mathbf{r}, \nu) \rangle_{\mathcal{R}}$ , between a dispersionless egression computation,  $\hat{H}_+$ , and surface amplitude,  $\hat{\psi}$ , averaged over a circular region of quiet Sun of radius 100 Mm, is plotted over the frequency range 2.5–6.5 mHz on successively finer scales proceeding from (a) to (d). The real part of the phase correlation is expressed by horizontal displacement and the imaginary part by vertical.

$$\check{G}_+(\mathbf{r}, \mathbf{r}', \nu) = f(|\mathbf{r} - \mathbf{r}'|) \exp(2\pi i \nu T(|\mathbf{r} - \mathbf{r}'|)) . \quad (22)$$

The effects of dispersion in the solar atmosphere can be estimated by computing quiet-Sun egressions,  $\check{H}_+(\mathbf{r}, \nu)$ , by the application of this dispersionless Green's function to Equation (4), and statistically correlating this with the surface amplitude,  $\check{\psi}(\mathbf{r}, \nu)$ , from which the egression was computed:

$$C(\nu) = \langle \check{H}_+(\mathbf{r}, \nu) \check{\psi}^*(\mathbf{r}, \nu) \rangle_{\mathcal{R}} . \quad (23)$$

Here we use angular brackets to express this statistical correlation as an average over a substantial domain,  $\mathcal{R}$ , over the solar surface.

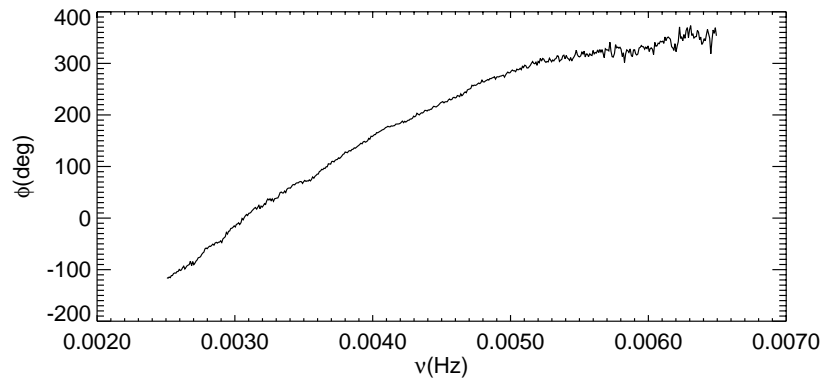


Figure 11. The phase of the correlation plotted in Figure 10 is rendered as a function of frequency over the range 2.5–6.5 mHz.

An example of such a measurement, averaged over some 17000 quiet-Sun pixels, is shown in Figure 10. In these plots, the real part of the correlation in each frame is the abscissa, with the imaginary part the ordinate. Because of the rapid attenuation in the acoustic power at the higher frequencies, the correlation must be plotted over a wide range of scales to cover the entire frequency band from 2.5–6.5 mHz. The phase,  $\phi(\nu)$ , of the correlation is plotted over this spectrum in Figure 11.

Dispersion can be viewed as primarily a result of the depth of the reflecting layer decreasing rapidly as frequency,  $\nu$ , increases. In fact, for the case in which  $\phi(\nu)$  has a constant slope, the effect is not actual dispersion of the wave packet but simply a temporal delay of the signature. It is the *curvature* of the locus of  $\phi$  that brings about actual temporal dispersion of a wave packet. In the case of Figures 10 and 11, the path of integration for travel time (see Equation (16)) was terminated 0.5 Mm beneath the photosphere, significantly beneath the reflecting layers for waves anywhere in the range 2.5–6.5 mHz. The resulting travel-time deficit significantly increases the slope of the locus of  $\phi$  plotted in Figure 11. It should be kept in mind that the loci plotted in Figures 10 and 11 represent *two* dispersive encounters with the surface, the first as the disturbance begins on its way into the solar interior from the surface, and the second on its return to the surface in the pupil. They are also sensitive to other factors beside dispersion and temporal errors. These include considerations of source depth distribution and the strong dependence of photospheric reflectivity on frequency. A reliable account for just dispersion may best be accomplished by a careful acoustic analysis of a realistic solar interior model.

Once dispersion and travel-time errors,  $\phi(\nu)$ , are known, these are easily corrected by simple multiplication:

$$\check{G}'_{+}(|\mathbf{r} - \mathbf{r}'|, \nu) = \check{G}_{+}(|\mathbf{r} - \mathbf{r}'|, \nu)e^{-i\phi(\nu)}. \quad (24)$$

Recent applications of seismic holography employing such a correction include the seismic imaging of a solar flare (Donea, Braun, and Lindsey, 1999), the study of the temporal properties of  $p$ -mode emission from acoustic glories and the quiet-Sun (Donea, Lindsey, and Braun, 2000), and phase sensitive holography of active regions (Braun and Lindsey, 2000b). In the formalism expressed by Equations (23) and (24) it is implicit that the correction,  $\phi$ , for dispersion depends only on frequency,  $\nu$ . For shallow sources surrounded by more compact pupils than those applied in the examples herein, this assumption introduces significant phase errors (Cally and Barnes, 2000). In that case, a more careful formalism expressing  $\phi$  as a function of  $(|\mathbf{r} - \mathbf{r}'|, z, \nu)$  is needed.

## 9. Summary

Our intention with this review has been to provide the most flexible introduction possible to the basic principles of solar acoustic holography. We hope to accommodate the reader who simply wants to be educated on a level that is as intuitive as possible. At the same time, this review should contain sufficient technical substance to be of practical service to readers interested in applying the technique to helioseismic observations. In fact, it is remarkably easy for the novice to compute high-quality phase-coherent images from publically available SOHO-MDI observations by following the basic guidelines expressed in this paper. The foregoing review has relied substantially on practical examples for this purpose. It is important that these should not be mistaken for a general prescription of ‘how to do’ seismic holography. Indeed, these examples do not begin to exhaust the concept, even in its present infancy. It should be understood that seismic holography was fashioned as a broad diagnostic generality that can and will be approached from any number of technical avenues, most of which are as yet untouched. The practical development and application of seismic holography is now at a most encouraging outset with the advent of SOHO and GONG. It is a little bit sobering to reflect that we are just beginning to enjoy with solar acoustics something that we have done habitually with electromagnetic radiation for eons in the application of our eyesight. How this new perspective will influence the direction of solar interior research is unpredictable, even in the near term. It will be very interesting indeed to see what new discoveries come out of solar acoustic holography over the next few years.

## Acknowledgements

We greatly appreciate the support our research has received from the SOHO SOI-MDI team and the fine quality of the data which they have given us. We especially appreciate the conscientious support of Dr P. Scherrer, head of the SOHO-MDI

project. SOHO is a project of international cooperation between ESA and NASA. D.C.B., a visitor at the Joint Institute for Laboratory Astrophysics, is grateful to Ellen Zweibel and the staff of JILA for their hospitality and support. The extraordinary dedication of our colleagues, particularly A.-C. Donea, M. Fagan, Y. Fan, Y. Gu, S. Jefferies, S. Redfield and M. Woodard, has been crucial to the successful development and fruitful application of solar acoustic holography over the past ten years. Solar acoustic holography was developed under grants from the National Aeronautics and Space Administration and from the Solar-Terrestrial and Stellar-Astronomy-and-Astrophysics branches of the National Science Foundation.

### References

- Born, M. and Wolf, E.: 1975a, *Principles of Optics*, Pergamon Press, Oxford, p. 375.  
 Born, M. and Wolf, E.: 1975b, *Principles of Optics*, Pergamon Press, Oxford, p. 424.  
 Born, M. and Wolf, E.: 1975c, *Principles of Optics*, Pergamon Press, Oxford, p. 425.  
 Born, M. and Wolf, E.: 1975d, *Principles of Optics*, Pergamon Press, Oxford, p. 300.  
 Born, M. and Wolf, E.: 1975e, *Principles of Optics*, Pergamon Press, Oxford, p. 113.  
 Braun, D. C. and Lindsey, C.: 1999, *Astrophys. J.* **513**, L79.  
 Braun, D. C. and Lindsey, C.: 2000a, *Solar Phys.* **192**, 285 (this issue).  
 Braun, D. C. and Lindsey, C.: 2000b, *Solar Phys.* **192**, 307 (this issue).  
 Braun, D. C., Duvall, T. L. Jr., and LaBonte, B. J.: 1988, *Astrophys. J.* **335**, 1015.  
 Braun, D. C., Lindsey, C., Fan, Y., and Jefferies, S. M.: 1992, *Astrophys. J.* **392**, 739.  
 Braun, D. C., Lindsey, C., Fan, Y., and Fagan, M.: 1998, *Astrophys. J.* **502**, 968.  
 Cally, P. and Barnes, G.: 2000, private communication.  
 Chang, H.-K., Chou, D.-Y., LaBonte, B., and the TON Team: 1997, *Nature*, **389**, 825.  
 Chen, H.-R., Chou, D.-Y., Chang, H.-S., Sun, M. T., Yeh, S.-J., LaBonte, B., and the TON Team: 1998, *Astrophys. J.* **501**, L139.  
 Chou, D.-Y., Chang, H.-S., Sun, M. T., LaBonte, B., Chen, H.-R., Yeh, S.-J., and the TON Team: 1999, *Astrophys. J.* **514**, 979.  
 Christensen-Dalsgaard, J., Proffitt, C. R., and Thompson, M. J.: 1993, *Astrophys. J.* **403**, L75.  
 Donea, A.-C., Braun, D. C., and Lindsey, C.: 1999, *Astrophys. J.* **513**, L143.  
 Donea, A.-C., Lindsey, C., and Braun, D. C.: 2000, *Solar Phys.* **192**, 321 (this issue).  
 Duvall, T. L. Jr., Jefferies, S. M., Harvey, J. W., and Pomerantz, M. A.: 1993, *Nature* **362**, 430.  
 Jiménez-Reyes, S. J., Régulo, C., Pallé, P. L., and Roca Cortés, T.: 1998, *Astron. Astrophys.* **329**, 1119.  
 Lindsey, C. and Braun, D. C.: 1990, *Solar Phys.* **126**, 101.  
 Lindsey, C. and Braun, D. C.: 1997, *Astrophys. J.* **485**, 895.  
 Lindsey, C. and Braun, D. C.: 1998a, *Astrophys. J.* **499**, L99.  
 Lindsey, C. and Braun, D. C.: 1998b, *Astrophys. J.* **509**, L129.  
 Lindsey, C. and Braun, D. C.: 1999, *Astrophys. J.* **510**, 494.  
 Lindsey, C., Braun, D. C., Jefferies, S. M., Woodard, M. F., Fan, Y., Gu, Y., and Redfield, S.: 1996, *Astrophys. J.* **470**, 636.  
 Messiah, A.: 1961, *Quantum Mechanics*, Wiley, New York, p. 231.  
 Roddier, F.: 1975, *Compt. Rend. Acad. Sci.* **281**, B993  
 Schlottmann, R. B.: 1999, *Geophys. J. Int.* **137**, 353.